Experimental behavior of piggy-backed anchors in the embedment stage and pull-out stage

H. Wu, Y. Lai*, B. Zhu
College of Civil Engineering and Architecture, Zhejiang University, China, wvhan@zju.edu.cn
laiying@zju.edu.cn (corresponding author), binzhu@zju.edu.cn

ABSTRACT: The drag embedment anchor is one of the most commonly used anchor types for the mooring systems of offshore floating structures. For the purpose of further enhancing the anchor efficiency, the piggy-backed anchors, connecting two drag embedment anchors in series, are evaluated in this study. This study presents the kinematic behaviors of two kinds of piggy-backed anchors in clay through laboratory experiments, including embedment tests and pull-out tests. The tests results, including anchor trajectory, incline angles and capacity, show that the piggy-backed anchors that the back of the front anchor's fluke is connected to the padeye of the rear anchor with a spacing of two fluke lengths exhibit the best capacity and rapid load response speed when subjected to in-plane and out-of-plane loads.

1 INTRODUCTION

In order to develop deep-sea resources, the safety of offshore floating structures must be prioritized, with particular attention to the selection of anchors for their mooring systems (Al-Umar et al., 2020; Liu et al., 2023; Wang et al., 2024). The drag-embedment anchor (DEA) is widely used in these mooring arrangements because it is simple to install and performs well across diverse seabed conditions. To improve anchoring performance further, the configuration of two DEAs linked in series—so-called piggy-backed anchors (see Figure 1)—has attracted growing interest (Lai et al., 2022; Chen et al., 2025; Lai et al., 2025).

When two DEAs are coupled to form piggy-backed anchors, the rear anchor can penetrate the seabed more deeply than a single anchor, and an appropriately designed linkage can generate a synergistic increase in bearing capacity that exceeds the simple sum of the two anchors (Lai et al., 2022). In contrast, inadequately designed connections may restrict the penetration of the front anchor or induce rotation of the rear anchor. Results from laboratory experiments and centrifuge modelling demonstrate that anchor spacing, attachment point, and plate aspect ratio are critical parameters governing the kinematic behavior of piggy-backed anchor systems (Lai et al., 2024; Chen et al., 2025).

Most existing research has concentrated on the behavior of piggy-backed anchors subjected to in-plane loads. In deep-water settings, however, extreme events such as hurricanes and tsunamis occur more frequently than in coastal regions, often damaging sections of mooring lines. As a consequence, the load transmitted to the remaining anchors may become eccentric relative to the plate centreline, resulting in out-of-plane (OOP) loading conditions (Benazir et al., 2023; Laksono et al., 2024; Liu et al., 2025). Such out-of-plane actions introduce torsional effects on the anchor, which diminish its ability to withstand vertical and in-plane horizontal forces, ultimately lowering the overall load-carrying capacity of piggy-backed anchor systems (Aubeny, 2018).

This study investigates the kinematic behavior of two kinds of piggy-backed anchors in the embedment stage and the pull-out stage, including anchor trajectory, incline angles and capacity. In the embedment stage, in-plane load was applied to anchors, and in the pull-out stage, in-plane and OOP loads were applied.

2 TEST SETUP

2.1 Loading apparatus

The cyclic loading apparatus (Figure 5) is employed in this study to conduct the embedment, cyclic and pull-out experiments, with two primary functions. Initially, uniform circular motion is performed by the rotation disk, which simulates the regular movement of the floating structures during their service life. The disk is actuated by a rotary servo motor capable of operating at rotational frequencies up to 0.3 Hz, and its maximum radius is 155 mm. In addition, the embedment and pull-out process are conducted when the anchor chain is retracted. The maximum load capacity of the apparatus is 6 kN.

2.2 Model anchor

Piggy-backed anchors connect two drag embedment anchors in series with the anchor chain. Two connection types are employed in this study (Figure 1), which are distinguished by the different attachment points. FB connection types, the back of the front anchor's fluke is connected to the padeye of the rear anchor with a spacing of two fluke lengths (L_f). PE conention types, the padeye of the front anchor is connected to the padeye of the rear anchor with a spacing of $2L_f$. A 4 mm diameter chain made of stainless steel was used in the tests, which followed standard usage guidelines (Vryhof, 2015). High-precision strain-gauge load cells (ZNLBM-50kg, 50 kg capacity; ZNLBM-20kg, 20 kg capacity) were used to monitor the tensions in the front and rear mooring lines. To reduce interference from soil sidewall friction, the cables were routed through the base, and the mooring lines were connected using coupling nuts. The entire assembly was then potted in epoxy resin to enhance sealing.

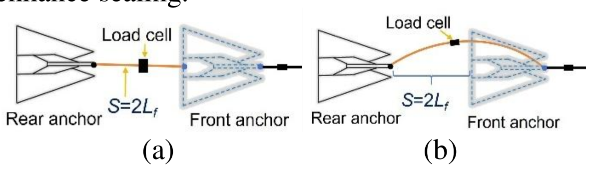

Figure 1. Connection types: (a). FB; and (b). PE

The model anchor (Figure 2), as a simplified version of DEA designed by Delmar Systems, Inc., which is fabricated from stainless steel and constructed at a 1:30 scale in comparison to the prototype. The anchor weight is 198 g, the fluke length (L_f) is 91 mm, the width (d_f) is 134 mm, the thickness (t_f) is 3 mm, and the area (A_f) is 6960 mm^2.

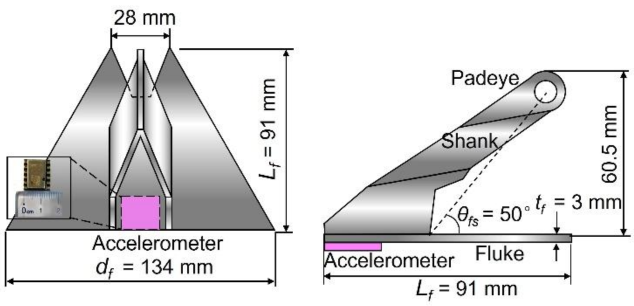

Figure 2. Model anchor

2.3 Accelerometer

The accelerometer was employed to record the orientations of the anchor: pitch (α), roll and yaw(θ). The rotation orientations of the anchor along the three coordinate axes have been specified, as illustrated in Figure 3. It is a cube with a side length of 15mm and a thickness of 3mm (Figure 2). Therefore, the friction generated by the accelerometer wire against the clay during embedding is minimal and can be disregarded in the drag anchor embedding process.

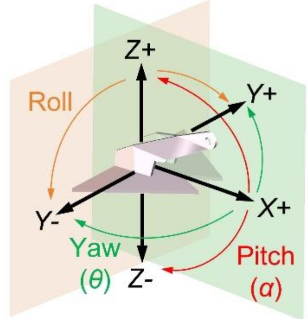

Figure 3. Orientation sign convention

The trajectory of the piggy-backed anchors is obtained through the integration method. The angles data are substituted into the Equations (1) to (3), and the position coordinates of the anchor at each moment can be calculated.

$$x = \int v \cdot \cos(d\alpha) \cdot \cos(d\theta)\, dt \qquad (1)$$

$$y = \int v \cdot \cos(d\alpha) \cdot \sin(d\theta)\, dt \qquad (2)$$

$$z = \int v \cdot \sin(d\alpha) dt \qquad (3)$$

where x, y, z is positional coordinates of the anchor; v is the anchor loading velocity (20 mm/s); α, θ is the pitch and yaw angles of the anchor, respectively.

2.4 Soil foundation

Malaysian kaolin was employed to prepare the saturated soft clay foundation due to its stable material properties, and it was widely used in scientific research (Lai et al., 2022; Chen et al., 2025; Lai et al., 2025). The preparation of the model soil bed followed the procedure described by Lee (2008). The undrained shear strength (s_u) was evaluated through a T-bar test, and the result is shown in Figure 4.

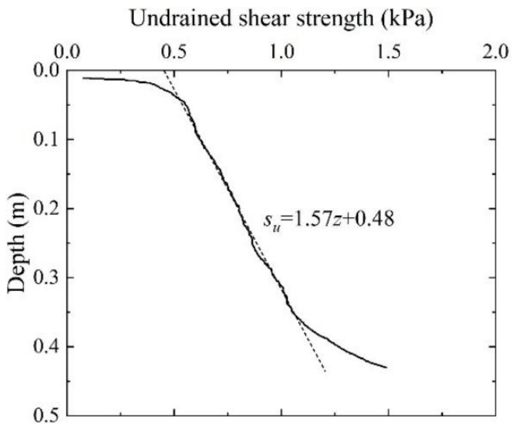

Figure 4. Shear strength profile

2.5 Experimental arrangement

Due to the limitations of the size of the model box (1.2 m × 0.95 m × 1.0 m), the whole tests were divided into two parts: (1) Embedment stage (Figure 5 (1)); and (2) pull-out stage (Figure 5 (2)). To eliminate boundary effects during loading, the anchor plate centroid was located 300 mm from the tank wall ($B_b/L_f > 3$), with a total foundation thickness of 500 mm ($5.5L_f$). These geometric parameters adhere to established guidelines for mitigating wall and base interference in anchor installation testing (Xu et al., 1997; Liu et al., 2010; Moore et al., 2021). Before the pull-out tests, the cyclic loading was conducted to simulate the motion of floating structures, with a radius of 30 mm and 200 cycles (Figure 6). In the embedment stage, the in-plane load was applied to piggy-backed anchors. In the pull-out stage, both the in-plane load and the out-of-plane (OOP) load were applied, with the OOP angles of 30° and 60°. In the pull-out stage, front anchor was embedded at $1L_f$ and the rear anchor at $2L_f$ in the piggy-backed anchors system, and the single DEA was embedded at $1.5L_f$ initially.

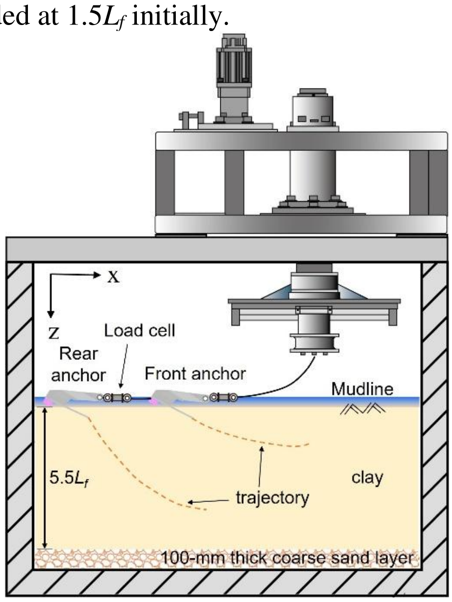

(a)

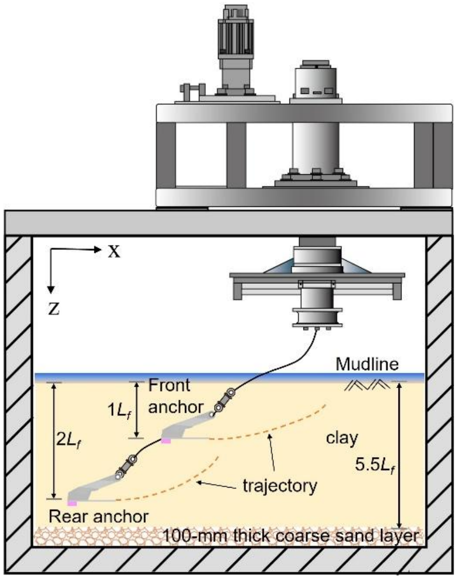

(b)

Figure 5. Experimental setup: (a) embedment stage; and (b). pull-out stage.

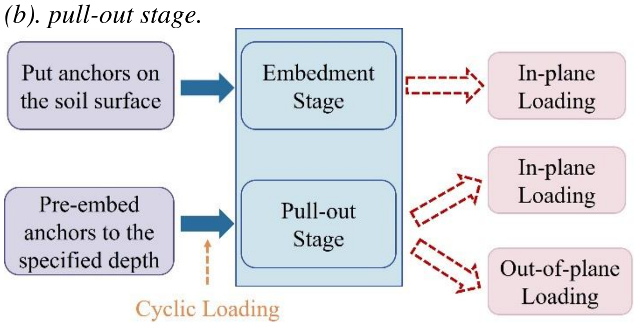

Figure 6. Flowchart of experimental arrangement.

3 RESULTS AND DISCUSSION

3.1 Embedment stage

In the embedment stage, in-plane load was applied to the single DEA and two types of piggy-backed anchors (FB and PE). Trajectory results reflect that the embedment depths of front anchors in two piggy-backed anchors system are approximately similar to the single anchor (Figure 7 (a)). However, rear anchors have a deeper embedment depth than that of the single anchor. In addition, the rear anchor of FB embeds more deeply than that of PE.

The pitch angle of the single anchor decreases most rapidly, the second is PE, and the slowest one is FB. The phenomenon illustrates that the fluke of the single anchor rotates most quickly, which explains why the embedment depth of the single anchor is the smallest and that of the FB is the largest.

Davis and Booker (1973) proposed a method for calculating the capacity factors, and capacity results in this study were normalized using this method. As shown in Figure 7 (c), with the largest embedment depth, FB yields the greatest capacity among three kinds of anchors.

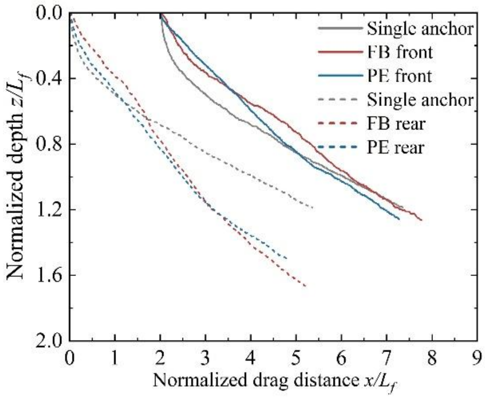

(a)

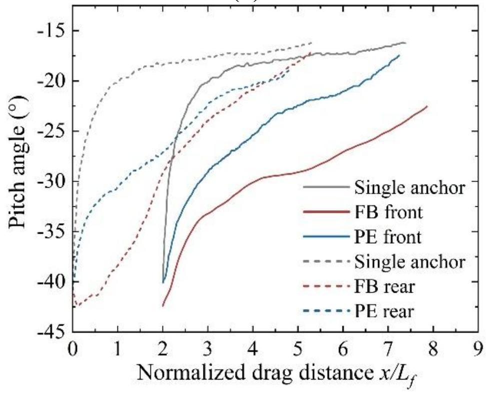

(b)

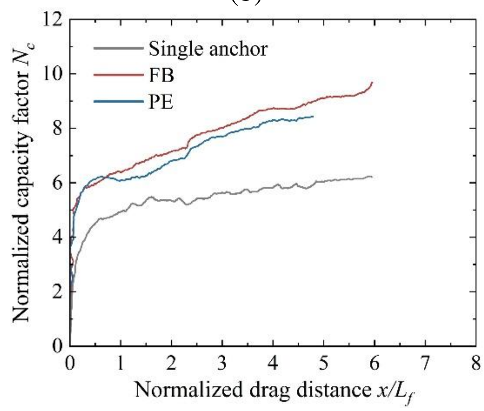

(c)

Figure 7. Embedment test results: (a). trajectory; (b). pitch angle; and (c). capacity.

3.2 Pull-out stage

In the pull-out stage, in-plane load and OOP load were applied to anchors. Two OOP angles are carried out here (30° and 60°).

3.2.1 In-plane loading

Embedment depth of PE decreases much more than that of the FB, this phenomenon occurs in both the front anchor and the rear anchor (Figure 8 (a)). The rear anchor uplift displacement of PE exceeds that of the single DEA.

Pitch angles results are aligned well with trajectory. Both anchors in PE system rotate more quickly than that of FB and single DEA. Therefore, PE shows a stronger pulling-out trend than other anchors. The reason is that, due to the configuration, the rear anchor of PE is attached to the padeye of the front anchor so that the fluke of the front anchor is free to rotate, whereas the front anchor of FB cannot. In addition, the configuration of PE causes the connecting chain to induce localized soil cutting, which weakens the soil wedge above the rear anchor and forms a disruption zone and makes the rear anchor rotate more easily.

Capacity of piggy-backed anchors is better than that of the single anchor. In addition, FB is better than PE, and the load response of FB is the fastest. Based on test results, FB demonstrates the robust bearing performance in the in-plane loading case.

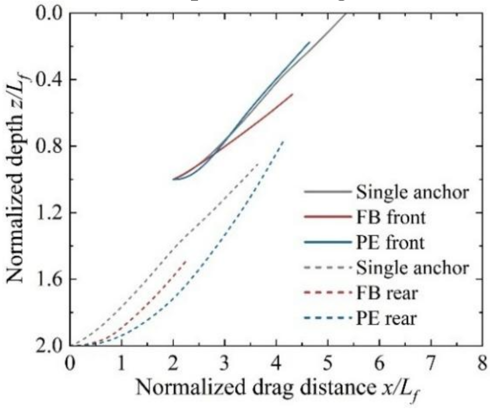

(a)

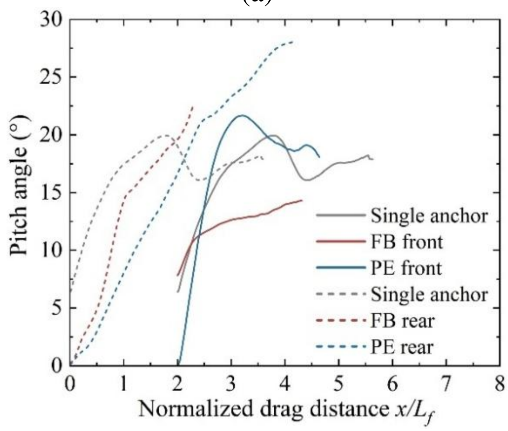

(b)

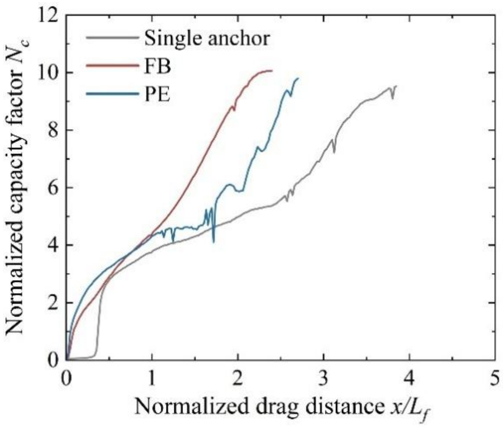

(c)

Figure 8. Pull-out test results under in-plane loading: (a). trajectory; (b). pitch angle; and (c). capacity.

3.2.2 Out-of-plane loading

As illustrated in Figure 9 (a), with the increase of OOP angles, the rate of the increase in the pitch angle of the front anchor is faster than that of the rear anchor. Therefore, the *xz*-plane projection of trajectory has the same trend of the changes. In addition, as shown in *xy*-plane projection of trajectory (Figure 9 (b)), the front anchor has a larger offset along the *y*-axis, which is aligned well with yaw angles results. In addition, even under nominally in-plane loading, small lateral movements can occur due to (1) spatial variability in the prepared soil bed (e.g., local density/strength non-uniformity), (2) slight deviations in anchor installation alignment and embedment condition, and (3) unavoidable system imperfections. The measured OOP behaviour was slightly disturbed by this inherent test uncertainty. However, residual lateral translation does not change the overall trend of the OOP response.

Capacity of FB decreases with the increase of OOP angles. This reduction arises from the greater moment and torsional demands, which diminish the portion of capacity available to resist vertical and in-plane horizontal loads (Zhao et al., 2020).

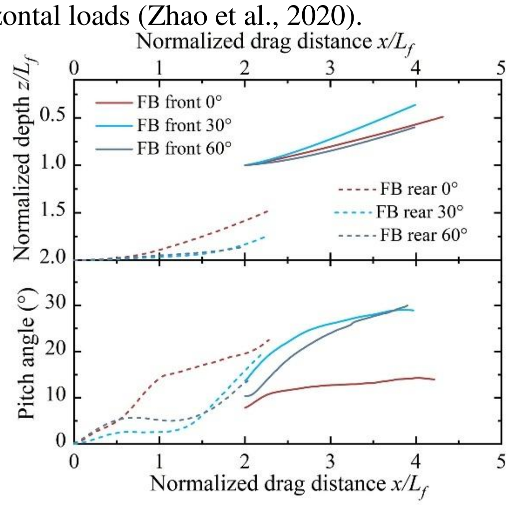

(a)

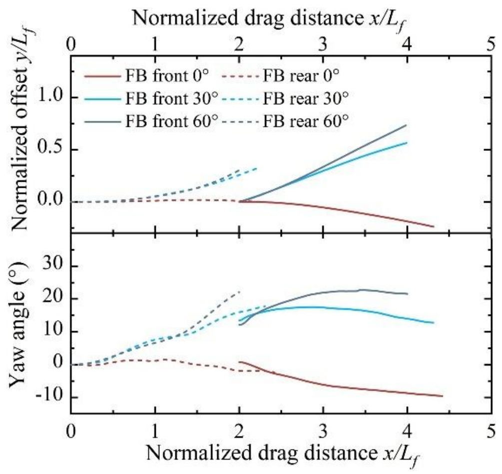

(b)

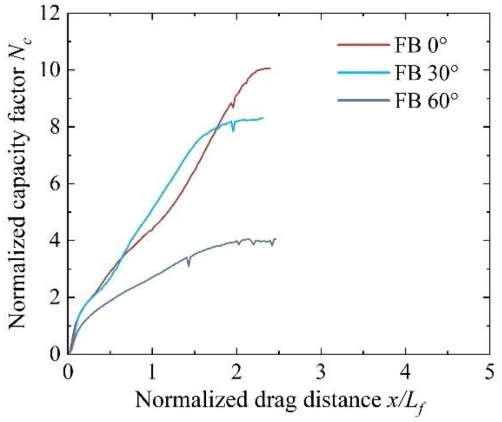

(c)

Figure 9. Pull-out test results under OOP loading for FB: (a). xz-plane projection of trajectory and pitch angle; (b). xy-plane projection of trajectory and yaw angle; and (c). capacity.

The uplift displacements of both the front anchor and the rear anchor for PE increase with the increase of OOP angles (Figure 10 (a)). The pitch angle of the front anchor increases initially and then decreases. The reason is that the front anchor is significantly affected by cyclic loads, the pitch angle increases quickly in the weak zone, and the growth rate decreases when the anchor drags into the normal consolidation zone. In addition, there exists a clear difference in yaw angle results between PE and FB. With the increase of OOP angles, the yaw angle of the rear anchor for PE increases more rapidly than that of the front anchor. This result indicates that the stability of rear anchor for PE is poor.

Capacity of the PE also decreases with the increase of OOP angles. There exists a two-stage development in capacity. This behavior arises from its unique connection configuration, which was mentioned in Section 3.2.1.

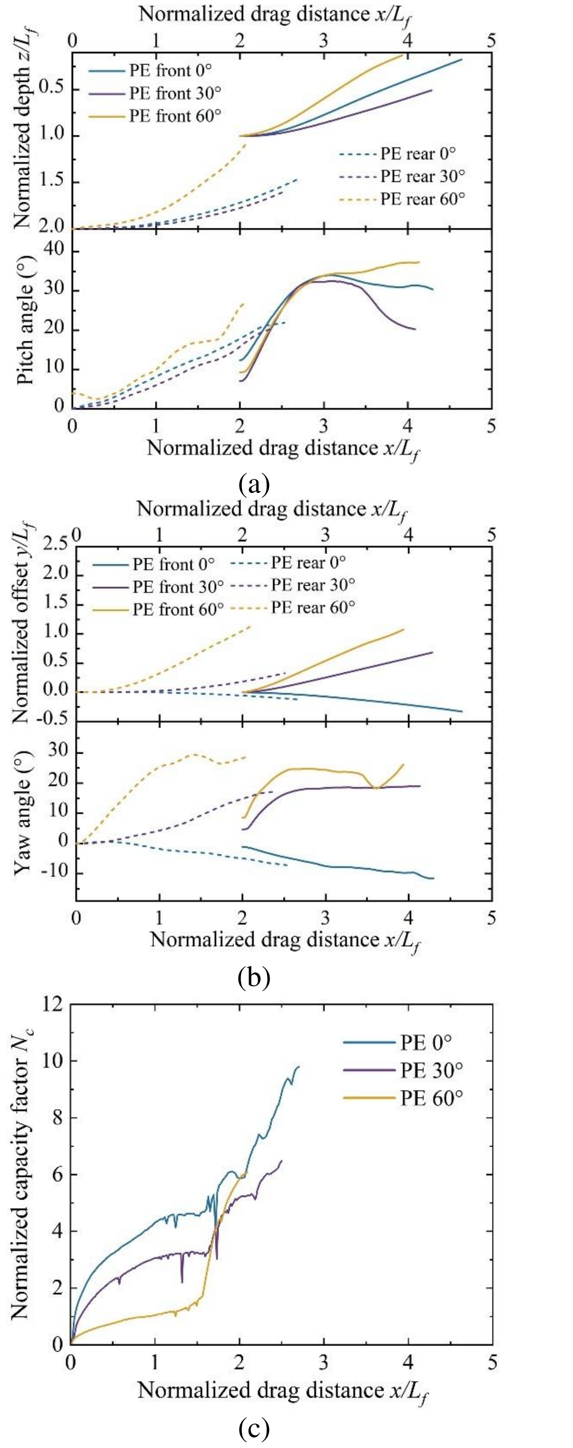

Figure 10. Pull-out test results under OOP loading for PE: (a). xz-plane projection of trajectory and pitch angle; (b). xy-plane projection of trajectory and yaw angle; and (c). capacity.

4 CONCLUSIONS

Embedment and pull-out tests are performed for two types of piggy-backed anchors (FB and PE) and the single anchor in this study. In the embedment stage, in-plane load was applied to anchors. In the pull-out stage, in-plane load and out-of-plane load were applied to anchors. The main conclusions are as follows: (1) In the embedment stage, the embedment depth of both front and rear anchors for FB is deeper than that of PE, and the capacity of FB is larger than that of PE. (2) In the pull-out stage, under in-plane loading, FB rotates slowly and has a smaller uplift displacement than PE, Therefore, FB has a relatively high safety margin. In addition, the load response speed of FB is faster. (3) In the pull-out stage, under out-of-plane loading, the capacity of anchors decreases with the increase of out-of-plane angles. There exists a two-stage development in capacity of PE. Besides, for FB, the yaw angle of front anchor is larger than that of the rear anchor, but for PE, it is the opposite. By comparing trajectory, angles and capacity of two piggy-backed anchors, FB (the back of the front anchor's fluke is connected to the padeye of the rear anchor with a spacing of two fluke lengths) has the better performance, with a higher capacity and a faster load response speed.

ACKNOWLEDGEMENTS

The fundings supported by the National Natural Science Foundation of China (No. 52522114, No. 52279112 and No. U23A20670) and Natural Science Foundation of Jiangsu Province (BK20241057) are gratefully acknowledged.

REFERENCES

Aubeny, C. (2018). *Geomechanics of marine anchors*. Florida: CRC Press, 27-28.

Lai, Y., Huang, Y., Gilbert, R., and Aubeny, C. (2022). The behavior of piggy-backed drag embedment anchors in marine soils. *Journal of Geotechnical and Geoenvironmental Engineering*, 148(1): 04021167. https://doi.org/10.1061/(ASCE)GT.1943-5606.0002713

Chen, H., Gao, Y., and Shu, S. (2025). Kinematic behaviors of piggy-backed vertically loaded anchors in clay. *Acta Geotechnica*, 20(4): 1859-1876. https://doi.org/10.1007/s11440-024-02482-x

Lai, Y., Chen, C., Yan, Z., and Zhu, B. (2024). The installation behavior and capacity of piggy-backed anchors for offshore wind turbine. *Sustainable Energy Technologies and Assessments*, 70: 103948. https://doi.org/10.1016/j.seta.2024.103948

Al-Umar, M., Fall, M., and Daneshfar, B. (2020). Gis-Based modeling of snowmelt-induced landslide susceptibility of sensitive marine clays. *Geoenvironmental Disasters*. 7(1). https://doi.org/10.1186/s40677-020-0142-8

Liu, X., Wang, Y., Zhang, H., and Guo, X. (2023). Susceptibility of typical marine geological disasters: an overview. *Geoenvironmental Disasters*. 10(1). https://doi.org/10.1186/s40677-023-00237-6

Wang, Z., Zheng, D., Guo, X., Gu, Z., Shen, Y., and Nian, T. (2024). Investigation of offshore landslides impact on bucket foundations using a coupled SPH–FEM method. *Geoenvironmental Disasters*. 11(1): 2. https://doi.org/10.1186/s40677-024-00266-9

Davis, E.H. and Booker, J.R. (1973). The effect of increasing strength with depth on the bearing capacity of clays. *Géotechnique*, 23(4): 551-563. https://doi.org/10.1680/geot.1973.23.4.551

Benazir, Syamsidik, Idris, Y., and Putra, N.P. (2023). Connecting community's perspectives on tsunami risk to anticipated future tsunamis: a reflection from a progress of tsunami preparedness from a coastal community in Aceh-Indonesia after 19 years of the 2004 Indian Ocean Tsunami. *Geoenvironmental Disasters*. 10(1): 18-21. https://doi.org/10.1186/s40677-023-00252-7

Laksono, F.X.A.T., Mishra, M., Mulyana, B., and Kovács, J. (2024). Exploring the mediterranean tsunami research landscape: scientometric insights and future prospects. *Geoenvironmental Disasters*. 11(1): 6. https://doi.org/10.1186/s40677-024-00269-6

Liu, K., Hsu, Y., Chen, Y., and Lin, Y. (2025). Deep sea water pumping pipe destruction due to undersea debris flow. *Geoenvironmental Disasters*. 12(1): 14. https://doi.org/10.1186/s40677-025-00319-7

Zhao, L., Bransby, M., and Gaudin, C. (2020). Centrifuge observations on multidirectional loading of a suction caisson in dense sand. *Acta Geotechnica*, 15(6): 1439-1451. https://doi.org/10.1007/s11440-020-00970-4

Xu, G. and Zhang, W. (1997). A review of model testing in the 2nd International Conference on Soft Soil Engineering. *Advances in Science and Technology of Water Resources*. (01): 40-43+60.

Liu, H., Zhang, W., and Zhang, X. (2010). Experimental investigation on the penetration mechanism and kinematic behavior of drag anchors. *Applied Ocean Research*. 32 (4): 434-442. https://doi.org/10.1016/j.apor.2010.09.004

Moore, E., Haigh, S., and Eichhorn, G. (2021). Anchor penetration depth in sandy soils and its implications for cable burial. *Ocean Engineering*. 235 (7): 109411. https://doi.org/10.1016/j.oceaneng.2021.109411

Lee, C. (2008). Constructing test bed of clay with a specified profile of undrained shear strength versus depth. M.S. Thesis. The University of Texas at Austin.

Vryhof A. Anchor manual. *Anchors Vryhof*; 2015.

Lai, Y., Xiong, S., Tao, P., Huang, C., Zhu, Q., Shu, S., and Chen, H. (2025). Experimental investigation and optimization of piggy-backed anchors in clay. *Ocean Engineering*. 333: 121513. https://doi.org/10.1016/j.oceaneng.2025.121513.